Korean J. Chem. Eng., 38(9), 1956-1969 (2021)
DOI: 10.1007/s11814-021-0837-x

pISSN: 0256-1115
eISSN: 1975-7220

Structurally ordered nanofiltration membranes prepared by spatially anchoring interfacial polymerization for highly efficient separation properties

Ao Sheng*, Hao Wang*, Haoji Jiang*, Yaxin Zhao*, Hao Li*, Hao Jia*, Zhong Wei*,,***,****,†, and Heyun Wang*,**,***,****,†**

*School of Chemistry and Chemical Engineering, Shihezi University, Shihezi 832003, China
**Key Laboratory for Green Processing of Chemical Engineering of Xinjiang Bingtuan, Shihezi 832003, China
***Key Laboratory of Materials-Oriented Chemical Engineering of Xinjiang Uygur Autonomous Region, China
****Engineering Research Center of Materials-Oriented Chemical Engineering of Xinjiang Bingtuan, China
(*Received 15 March 2021 • Revised 30 April 2021 • Accepted 3 May 2021*)

Abstract−The incorporation of various nanofillers into the interfacial polymerization (IP) process is widely applied to prepare higher performance NF membranes. However, few studies have reported the influence of nanofillers on nanocomposite membrane formation in the IP process. Here, an optical microscope was employed to study the change rule in the 8-NH_2-POSS/PSA nanocomposite membrane formation process due to the addition of 8-NH_2-POSS nanoparticles. First, the addition of 8-NH_2-POSS reduced the diffusion rate of the polyacrylamide hydrochloride (PAH) water phase on the surface against the oil phase because of the interaction with the PAH molecules. Furthermore, the 8-NH_2-POSS/PSA nanocomposite membrane structure was more homogeneous and exhibited uniform pinhole defects distribution due to the interaction of the 8-NH_2-POSS nanoparticles to the PAH segment. A significant separation performance was observed in the 8-NH_2-POSS/PSA nanocomposite membrane due to the hydrophilicity and positive charge of the 8-NH_2-POSS nanoparticles. The permeation flux and $MgCl_2$ rejection of the 8-NH_2-POSS/PSA nanocomposite membrane increased up to 50.5 L/m^2 h at 0.5 MPa and 94.8%, respectively, which corresponded to increases of 73.5% and 8.7% as compared to the pristine PSA membrane. 8-NH_2-POSS/PSA nanocomposite membranes have great application potential in the water softening and treatment of divalent metals ions under acidic conditions.

Keywords: 8-NH_2-POSS Nanoparticles, Interfacial Polymerization, NF Nanocomposite Membrane, Membrane Formation Process, Separation Performance

INTRODUCTION

Water shortage has become a global issue with the growth of the global population, continuous development of the industry, increasing range of pollution, and the declining quantity of clean water. In general, industrial wastewater is hugely harmful to organisms, such that the treatment of industrial wastewater has been prioritized in recent years. To solve global water problems, numerous studies have explored economic and efficient technologies for sewage treatment. Nanofiltration (NF), which is energy-saving, highly selective, and compatible with other separation processes, has been widely applied for sewage treatment and other industries over the past few decades [1-3]. In particular, for nanofiltration process, the preparation of the nanofiltration membranes is an important parameter. Currently, NF membrane preparatory methods can be roughly divided into the following categories: interfacial polymerization [2], layer-by-layer self-assembly [4], surface grafting [5], and physical coating [6,7]. In particular, interface polymerization (IP) is widely used commercially due to its convenience, efficiency, and stability [8,9]. However, the most commonly used commercial NF membranes are prepared via interfacial polymerization, such as polyamide (PA) composite membranes, which has low flux and selectivity, though this does not overcome the "trade-off" effect.

In general, the permeation flux of NF membranes is mainly determined by two aspects: (1) the adsorption of water molecules onto the membrane surface, and (2) the diffusion of water molecules in the membrane. Therefore, it is feasible to improve the permeation flux of water by improving these two aspects of membrane materials. At present, embedding some nanomaterials in the polymer to prepare nanocomposite membranes has proven to be an effective way to improve the membrane performance [10,11]. To date, many nanomaterials, such as zeolite 4A [12], titanium dioxide [13], graphene oxide (GO) [14,15], carbon nanotubes (CNTs) [16], metal organic frameworks (MOFs) [17], and covalent organic frameworks (COFs) [18], have been successfully incorporated into the polymer to prepare nanocomposite membranes with better separation performance as compared to the original membrane. However, the addition of nanomaterials to the membrane produces poor dispersion in the water phase and poor compatibility with the polymer matrix, which may result in non-selective defects on the membrane surface to reduce the stability and the separation performance of the membrane. Therefore, many researchers have tried some methods, such as reducing nanomaterial sizes, hydrophilic modification, or selecting hydrophilic nanoparticles, to enhance the dispersion of nanoparticles in the water phase and the compatibility of nanoparticles with polymers. Bruggen et al. prepared a new thin film nanocom-

†To whom correspondence should be addressed.
E-mail: steven_weiz@sina.com, whyun@shzu.edu.cn
Copyright by The Korean Institute of Chemical Engineers.

posite nanofiltration membrane (TFN) by adding cellulose nanoparticles (CNCs) to the interfacial polymerization reaction of polyethyleneimine (PEI) and trimesoyl chloride (TMC). The CNCs exhibited granular protrusions on the membrane surface, which greatly increased the surface roughness. Increased CNC content greatly improved the water flux of the TFN membranes, though its rejection rate dropped. Although increased roughness is conducive to increased water flux, the addition of CNCs affects the interface polymerization reaction rate of PEI and TMC, which can result in a loose membrane structure as well as a drop in the rejection rate [19]. Zhang et al. developed new TFN membranes by the interfacial polymerization of poly(sodium 4-styrenesulfonate) (PSS) modified ZIF-8 (mZIF), TMC, and piperazine (PIP). By coating the surface of the ZIF-8 nanoparticles with a layer of PSS, mZIF exhibited good dispersion in the water phase and interface compatibility. Better mZIF-8 wetting with anionic PSS resulted in increased PIP monomer adsorption on its surface to form polyamide tufts. The non-isotropic tufts and lateral diffusion of PIP can produce a rough net-like structure, which would ultimately generate a volcano-like structure [17]. Mansourpanah et al. embedded triethylenetetramine-modified graphene oxide (GO-TETA) into the PA-TFN membrane to greatly improve its hydrophilicity, antifouling, rejection, and water flux. Following the addition of GO-TETA, a smoother membrane surface and greatly reduced roughness were observed. These surface effects are believed to be caused by the following three reasons: (1) GO-TETA may be placed horizontally along the membrane surface, thereby inhibiting PIP diffusion; (2) hydrogen bonding was observed between GO-TETA and functional groups of PA membrane; and (3) larger GO-TETA sizes reduced possible cross-linked structure growth for PIP and TMC, resulting in a smoother PA membrane [20]. However, this explanation for changes of membranes is limited to the inference of the atomic force microscopy (AFM) and scanning electron microscopy (SEM) results without additional substantive proof. The influence of the fillers on the surface morphology and roughness of the composite membrane is still ambiguous.

The separation performance significantly affects the membrane structure. However, the influence of the hydrophilic nanoparticles on the formation of the nanocomposite membrane has been minimally reported. It is of vital importance to understand the formation process to improve the performance and applicability of the nanocomposite membrane prepared via the IP process. To study the membrane formation in the IP process, Wang et al. employed an optical contact angle measuring device (OCA) to monitor changes in the interface morphology of the water phase drop in the oil phase, and membrane formation during the interfacial polymerization process [21]. This study demonstrates a very useful method for studying the fundamentals of the IP membrane formation.

Until now, few studies have reported the influence of the addition of hydrophilic nanoparticles on the IP process. This work is an attempt to fill this gap. Specifically, we selected polysulfonamide (PSA) prepared in our past work as the substrate membrane and hydrophilic 8-NH_2-polyhedral oligomeric silsesquioxane (8-NH_2-POSS), which has an abundance of amino groups, a small size (1-3 nm), and high compatibility and dispersion [22-24], as the filler to prepare the 8-NH_2-POSS/PSA nanocomposite membrane. To better simulate the IP process, an optical microscope was used to observe the IP process in real time on the horizontal interface. The influence of the different additions of 8-NH_2-POSS on the IP process was examined and the changes in the surface topography were characterized. The desalination properties of the PSA nanocomposite membranes with the different additions of 8-NH_2-POSS were also discussed.

MATERIALS AND METHODS

1. Materials

Polyethersulfone (PES, MW=30,000 Da) was supplied by Beijing ZhongKe RuiYang Technology Co., Ltd. Polyacrylamide hydrochloride (PAH, powder, MW=17,500 Da, purity 98%) and 1,3-benzenedisulfonyl chloride (BDSC, purity 98%) were provided by Sigma-Aldrich. Octa Ammonium polysilsesquioxane (8-NH_2-POSS) was supplied by HuNan Chang Sha Ba Xi Technology Co., Ltd. Isopar G was supplied by the GuangDong Tikom Company. 4-Dimethylaminopyridine (DMAP) and sodium dodecyl sulfate (SDS) were supplied by the China ShanTou Xi Long Chemical Factory.

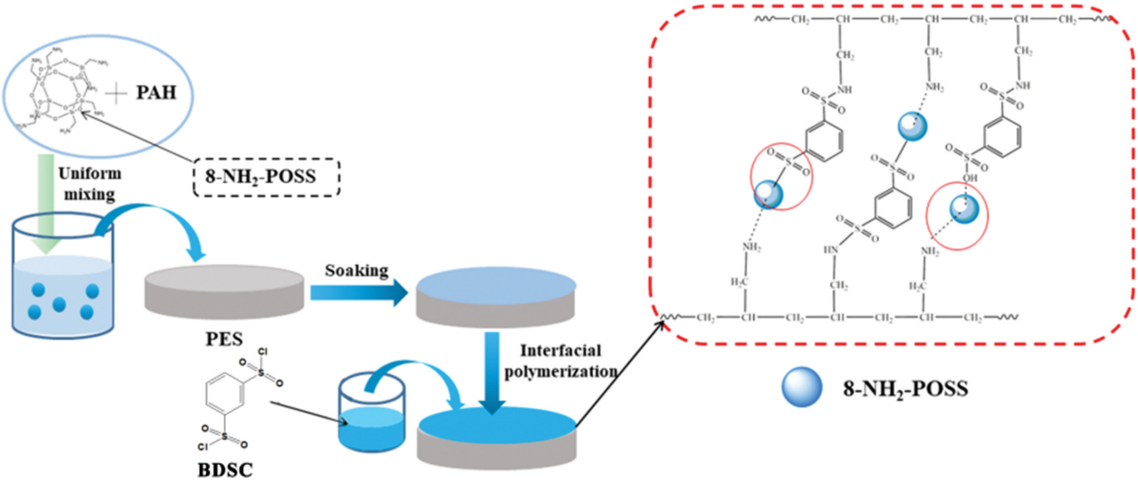


Fig. 1. Preparation process of the 8-NH_2-POSS/PSA nanocomposite membrane.

Table 1. 8-NH_2-POSS/PSA nanocomposite membranes at different 8-NH_2-POSS contents

Membranes	PAH (w/v%)	BDSC (w/v%)	8-NH_2-POSS
P-0	0.8	0.15	0
P-1	0.8	0.15	0.1
P-2	0.8	0.15	0.3
P-3	0.8	0.15	0.5
P-4	0.8	0.15	0.7
P-5	0	0.15	0.7

Polyethylene glycol (PEG Mw=200, 400, 800, 2,000, 4,000, 6,000, and 10,000 Da) was supplied by Macklin.

2. Preparation of the 8-NH_2-POSS/PSA Nanocomposite Membrane

Fig. 1 shows the preparation process of the 8-NH_2-POSS/PSA nanocomposite membrane. The detailed preparation steps are as follows: First, the PES support layer was immersed in deionized (DI) water for 24 h and then dried. Second, a certain amount of PAH, 8-NH_2-POSS (Table 1), DMAP (0.2 w/v%) as the catalyst and SDS (0.025 w/v%) were dissolved in deionized water to prepare the aqueous solution. The pH was adjusted to 9.35 using a NaOH solution. The PES support layer surface was then soaked in the aqueous solution for 20 min to remove excess PAH coating support layer on the solution surface and dried until no liquid was observed at room temperature. Third, the PAH-coated support layer surface was soaked in a organic phase solution of BDSC for 20 min. The excess solution was then expelled and the initial membrane was heated at 95 °C for 10 min. Finally, the newly acquired 8-NH_2-POSS/PSA nanocomposite membrane was stored in deionized water until testing.

3. Effects of the Nanoparticles on the Interfacial Polymerization Process

The experiments were performed at room temperature (25 °C). Since the interfacial polymerization reaction of the membrane occurs on a plane, an optical microscope (OLYMPUS BX53, Japan) was used to observe the IP process to better simulate the situation. A PAH water phase (10 mL) was doped with different amounts of 8-NH_2-POSS (P-0, P-1, P-2, P-3, P-4, P-5) and a BDSC oil phase (10 mL) was injected into the ultra-flat petri dish. The IP process was recorded using an optical microscope (Olympus BX53, Japan). The changes in the bubble size on the membrane surface across different time periods were tested using ImageJ software (the average bubble size of 100 data points was recorded across five different regions and averaged). The interfacial tension of the aqueous droplets was measured using the hanging drop method with a contact angle surface tension meter (Kruss Easy Drop Goniometer, Germany).

4. Characterization of the 8-NH_2-POSS/PSA Nanocomposite Membrane

Before characterization, the membranes were dried under a vacuum at 25 °C for 24 h. The surface and cross-sectional morphology of the membrane were analyzed by scanning electron microscope (SEM) (U8020, Japan). Atomic Force Microscopy (AFM) (Mutilmode 8, Germany) was used to analyze the surface roughness of the membrane. Attenuated total reflectance-Fourier transform infrared spectroscopy (ATR-FTIR) (Bio-Rad FTS-6000, USA) and X-ray photoelectron spectroscopy (XPS) (PerkinElmer PHI 5000C ESCA System, USA, Mg Kα1, 2 radiation source) were used to analyze the surface chemical functionality of the membranes. The surface hydrophilicity of the membranes was analyzed using a water contact angle (WCA) goniometer (Kruss Easy Drop Goniometer, Germany) at room temperature, wherein the WCA data was obtained from the average of six different positions on the membrane surface. The spectrum was obtained in the range of 0 to 1,200 eV. The surface zeta potential of the membrane was analyzed by an electric analyzer (Anton Paar Gmbh, Austria). The electric analyzer was measured using KCl (1 mmol/L) as the electrolyte solution. The pH of the electrolyte solution was adjusted using NaOH and HCl solutions.

5. Performance Evaluation of the 8-NH_2-POSS/PSA Nanocomposite Membrane

The separation performance of the 8-NH_2-POSS/PSA nanocomposite membrane was evaluated by a homemade cross-flow flat membrane system. The cross-flow flat membrane system measured an effective membrane area (12.56 cm^2). Each membrane was pre-pressed with 0.6 MPa of pure water for 2 h, after which the membrane properties were evaluated. An inorganic salt solution (NaCl, Na_2SO_4, $MgSO_4$, $MgCl_2$) and a PEG solution were used as the feed solutions for a 0.5 MPa permeation test at room temperature. Additionally, to ensure repeatability, the performance results of the test were the average of more than three samples from each kind of membrane. The permeate flux (F, L/m^2h) and rejection (R, %) of the membrane were calculated as follows:

$$F = \frac{V}{At} \tag{1}$$

$$\text{Permeate} = \frac{F}{\Delta P} = \frac{V}{At\Delta P} \tag{2}$$

$$\Delta P = P - \pi = P - (i\Delta MRT) \tag{3}$$

where V is the permeate volume (L); A is the membrane area (m^2); t is the filtration time (h); ΔP represents the effective transmembrane pressure; P represents the actual pressure (MPa); π represents the osmotic pressure; M is the molar difference (mol/ L) of the solute between the feed and the permeate; i is the van't Hoff factor of the relevant solute; R is the common gas constant (0.08314 L bar mol^{-1} K^{-1}); and T is absolute temperature (K).

Rejection (R, %) of the membrane was calculated as follows:

$$R = \left(1 - \frac{C_p}{C_f}\right) \times 100\% \tag{4}$$

where the C_p and C_f represent the solute concentrations (g/L) of the permeate and feed solution, respectively.

The MWCO of the membrane was evaluated using a different molecular weight PEG solution with uncharged properties. The Donnan Steric Pore model (DSPM) was used to calculate the membrane pore size. Thus, the rejection of uncharged solutes was calculated as follows [25,26]:

$$R_p = (1 - \Phi K_{i,c}) \times 100\% \tag{5}$$

$$\lambda = \frac{r_i}{r_p} \quad (6)$$

$$\Phi = (1-\lambda^2) \quad (7)$$

$$K_{i,c} = (2-\Phi)(1.0+0.054\lambda-0.988\lambda^2+0.441\lambda^3) \quad (8)$$

The empirical relationship based on molecular weight (MW, Da) was defined as follows [25]:

$$\log r_i = -1.3363+0.395 \log M_W \quad (9)$$

where R_p, Φ, $K_{i,c}$, λ, r_p, r_i, and M_W define the solute repulsion, spatial partition coefficient, space barrier factor, ratio of the solute radius to the pore radius, pore radius (nm), solute radius (nm), and numerator weight (Da), respectively.

The PEG concentration data were collected by spectral titration [27]. A DDSJ-307A conductivity meter (Shanghai Leichi Instruments, China) was used to measure conductivity to obtain salt concentration data. The acid stability of the membrane was evaluated using previously developed methods [28]. The detailed procedure is as follows: First, the membrane was exposed to a H_2SO_4 solution (20 w/v%) at room temperature (25 °C) for a fixed period of time. Next, the membrane sample was taken out of the acidic solution and washed with deionized water. Finally, the membrane samples were placed in deionized water until testing.

RESULTS AND DISCUSSION

1. Optimization of the Preparation Conditions of the 8-NH_2-POSS/PSA Nanocomposite Membrane

The preparation conditions of the membrane were optimized to minimize external influences, such as the PAH and BDSC concentrations, on interfacial polymerization [29]. Herein, the effects of the PAH and BDSC concentrations on the membrane separation performance were respectively studied to determine the optimal concentration of the reactive monomer.

First, we showed the effect of PAH concentration on the separation performance of the 8-NH_2-POSS/PSA nanocomposite membrane (Fig. 2). As shown, the concentration of 8-NH_2-POSS and BDSC are fixed at 0.1 w/v% and 0.1 w/v%, respectively. With the increase of the PAH concentration from 0.3 w/v% to 0.8 w/v%, the water permeability flux decreased from 51.6 L/m^2 h to 35.2 L/m^2 h. Similarly, the interception rate of $MgCl_2$ increased from 62.8% to 80.3%. However, further increase of the PAH concentration to 1.2 w/v% resulted in a water permeability flux increase to 38.6 L/m^2 h and a $MgCl_2$ retention rate decrease to 76.2%. It is possible that the increase from a low PAH concentration resulted in a decrease in the membrane water permeability flux and an increase in the $MgCl_2$ retention rate. This trend was consistent with those previously reported by Chung's et al. [30]. However, with the further increase of the PAH concentration, the water permeation flux of the membrane increased and the retention rate of $MgCl_2$ sharply decreased possibly because PAH with low diffusion rate into the organic phase did not readily react with BDSC. Thus, the BDSC organic monomers diffused into the aqueous phase and reacted with PAH. At a high PAH concentration, a significant number of amino groups were present on the PES base membrane to provide reaction sites. In this case, the number of sulfonyl chloride groups in BDSC was in short supply as compared to the amino groups, such that the degree of reaction between the two groups was low. Therefore, the active separation layer of the formed 8-NH_2-POSS/PSA nanocomposite membrane was relatively loose and thus exhibited a high water permeability flux and low salt retention rate. According to the above experimental results, the optimal concentration of PAH was 0.8 w/v%.

Previous studies characterized the influence of the BDSC concentration on the separation performance of the 8-NH_2-POSS/PSA nanocomposite membrane. According to Fig. 3, the concentrations of PAH and 8-NH_2-POSS were 0.8 w/v% and 0.1 w/v%, respectively. As the concentration of BDSC increased from 0.05 to 0.15 w/v%, the water permeability flux decreased from 43.1 L/m^2 h to 34.3 L/m^2 h, and the interception rate of $MgCl_2$ increased from 68.6% to 89.5%. As the BDSC concentration further increased to 0.2 w/v%, the interception rate of $MgCl_2$ slightly changed, while

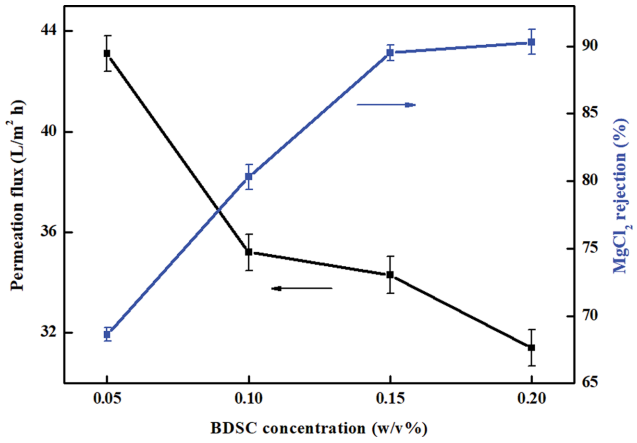


Fig. 2. Effect of BDSC concentrations on the separation performance of the 8-NH_2-POSS/PSA nanocomposite membrane evaluated with a 1 g/L $MgCl_2$ solution, at 0.5 MPa, and at room temperature (25 °C).

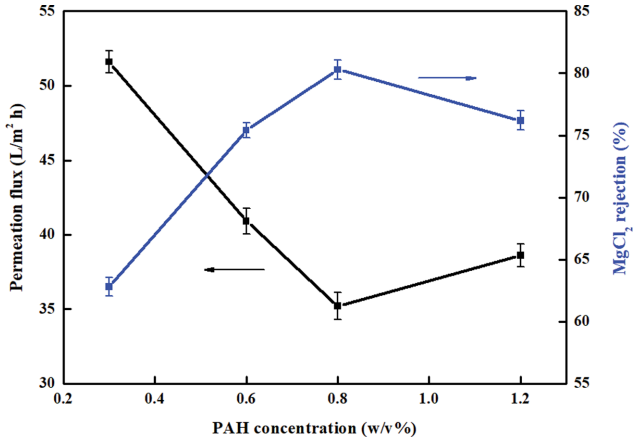


Fig. 3. Effect of the PAH concentration on the separation performance of the 8-NH_2-POSS/PSA nanocomposite membrane evaluated with a 1 g/L $MgCl_2$ solution, at 0.5 MPa, and at room temperature (25 °C).

the water permeation flux decreased to 31.4 L/m^2 h. This change in trend was consistent with the influence of BDSC on the PSA membrane we reported. The organic monomer concentration was positively correlated to the degree of interfacial polymerization, such that an increase in the concentration resulted in the formation of a dense and thick 8-NH_2-POSS/PSA active separation layer. The produced 8-NH_2-POSS/PSA nanocomposite membrane thus exhibited a low water permeability flux and high salt retention rate. According to the above experimental results, the optimal concentration of BDSC was 0.15 w/v%. The above experiments systematically studied the influence of the concentration of PAH and BDSC on the membrane separation performance. The optimal concentrations of PAH and BDSC were determined to be 0.8 w/v% and 0.15 w/v%, respectively.

2. Effects of the 8-NH_2-POSS Nanoparticles on the Interfacial Polymerization Process

The IP method is based on a polycondensation reaction on the organic side of the interface between two monomers dissolved in immiscible solvents. The 8-NH_2-POSS nanoparticles were added into the PAH water phase, thereby creating a change in the surface tension of the PAH aqueous solution following the addition of different amounts of 8-NH_2-POSS nanoparticles, which were measured using the pendant drop method. According to the results in Fig. 4, the surface tension of the PAH aqueous solution significantly increased from 10.37 mN/m to 20.46 mN/m under the 0.5 wt% content of 8-NH_2-POSS. The surface tension did not present any significant changes with the continuous addition of 8-NH_2-POSS. The increment of surface tension indicated a strong interaction in the water phase following the addition of the 8-NH_2-POSS nanoparticles. The strong interaction in the water phase would inevitably affect the mass transfer in the IP process.

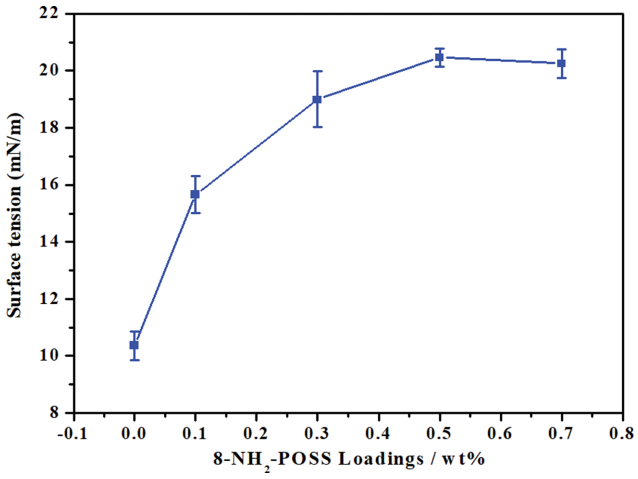


Fig. 4. Surface tension changes at different 8-NH_2-POSS loadings.

Optical microscopy (OM) is a very useful tool to examine the fundamentals of the IP membrane formation process in situ. Fig. 5 illustrates the variation of the composite membrane surface morphology with the different 8-NH_2-POSS content at different IP process times. According to Fig. 5, some bubble-structure rapidly appeared within 1 min, indicating an immediate chemical reaction on the interface. Little bubbles appeared to fuse into a big bubble at prolonged times. The bubble size decreased with the addition of 8-NH_2-POSS. It should be noted that the bubbles were solidified on the membrane.

To clearly observe the variations of the cells, the cellular size was calculated by Image J software, as shown in Fig. 5; the results are summarized in Fig. 6. According to Fig. 6, with increasing time,

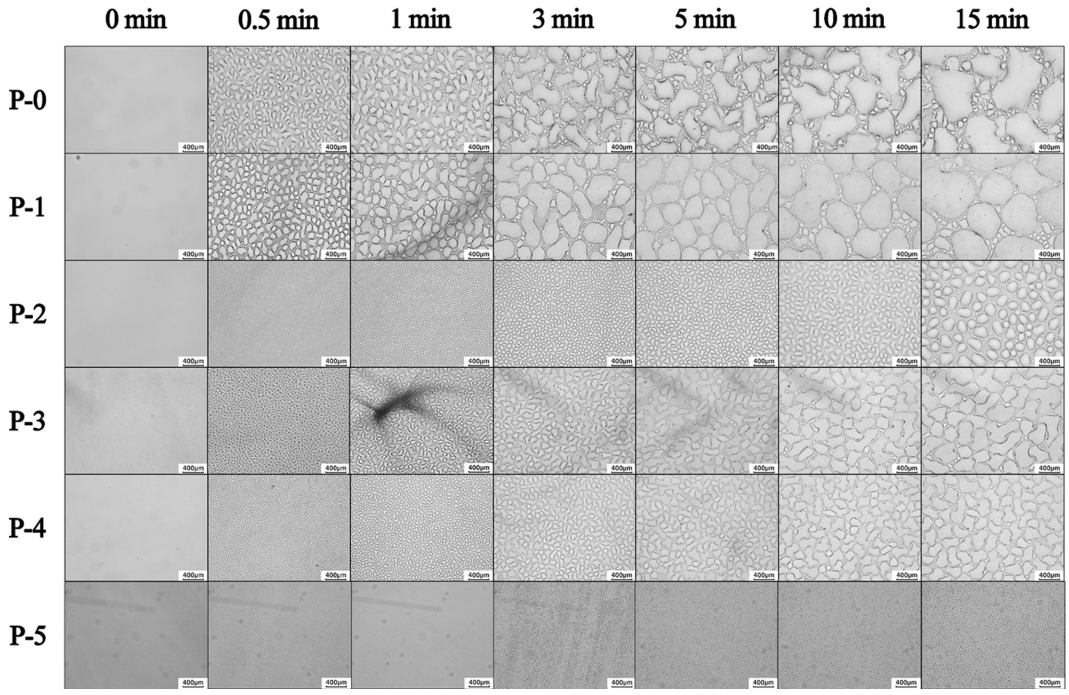


Fig. 5. Nanocomposite membrane surface morphology at different 8-NH_2-POSS contents at various times across the IP process.

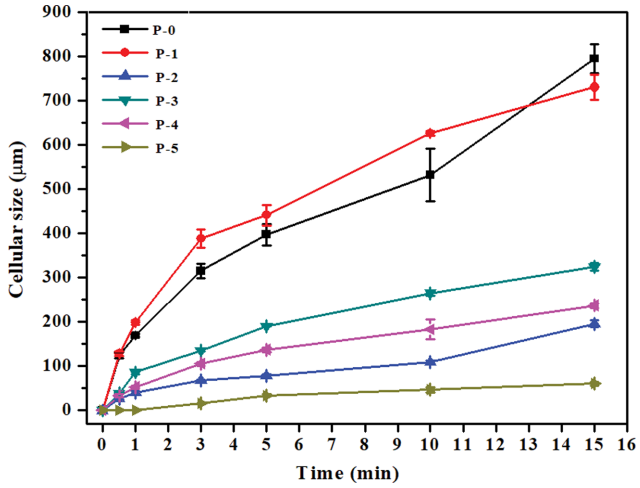


Fig. 6. Cellular size versus time; the cellular size was calculated from Fig. 5.

the bubble size increased rapidly without the 8-NH_2-POSS nanoparticles or with 0.1 wt% content of 8-NH_2-POSS. In comparison, the bubble size slowly increased at 8-NH_2-POSS contents over 0.3 wt%. P-5 was used as a reference, to which a rate of bubble formation was not observed. The formation and variation of the bubbles may be explained as follows. After the contact of the PAH water phase and BDSC organic phase, interfacial polymerization immediately occurred and formed a nascent membrane with the pinhole that was insoluble in any phase at the aqueous-organic interface. Therefore, the PAH molecules in the water phase could diffuse through the pinhole defects into the BDSC organic phase for further reaction. Some drops of the water phase coalesced and resulted in polymer precipitation at the drop-organic interface, thereby forming a new membrane with bubble. The newly formed bubbles covered the previously formed bubbles, which resulted in little bubble combinations that eventually formed a new bigger bubble with increasing time. Finally, it was more difficult for the PAH molecules to diffuse into the BDSC organic phase as the reaction progress until a somewhat constant bubble size was maintained with the increasing time. Notably, the size and size distribution of the bubbles were obviously different with the addition of 8-NH_2-POSS.

Based on this phenomenon, a possible membrane formation process was proposed in IP with the addition of 8-NH_2-POSS. First, PAH water phase came into contact with the BDSC oil phase to form a thermodynamically unstable nascent membrane with uneven pinhole defects, which generated a different PAH molecular diffusion rate in the water phase on the surface as compared to the BDSC oil phase. Eventually, a PSA membrane with a bubble-like coarse structure was obtained. As an octa amino cage nanoparticle, 8-NH_2-POSS has spatially distributed amino groups that can form strong hydrogen bonds with the water molecules and present a very slow diffusion rate from the water phase to the oil phase (P-5). Therefore, it could move with water molecules in the water phase instead of depositing in the water phase. The 8-NH_2-POSS and PAH molecules can also form molecular interactions and influence the diffusion of the PAH molecules to the organic phase. At very low 8-NH_2-POSS addition (below 0.3 w/v%), the surface tension of the PAH water phase was too weak to influence the diffusion rate of the PAH molecules to the organic phase. The rapid diffusion of the PAH molecules resulted in a nascent membrane on the oil phase being unstable with many unevenly distributed pinholes. As a result, non-uniform diffusion of the PAH molecules to the BDSC organic phase on the surface of the nascent membrane was observed, thus generating a second generation membrane with different sizes bubbles and many unevenly distributed pinholes. Finally, bubbles with particularly inconsistent sizes and distributions were observed on the final membrane, which resulted in membrane defects and high surface roughness. The surface tension of the PAH water phase increased with the addition of 8-NH_2-POSS, and the interfacial tension between the nascent membrane and organic solvent also increased with the addition of 8-NH_2-POSS. The increase in the interfacial tension between the nascent membrane and organic phase reduced the instability of the nascent membrane, thus forming evenly distributed pinholes on the nascent membrane and producing smaller bubbles on the membrane. Therefore, all the secondary membranes exhibited bubbles with uniform

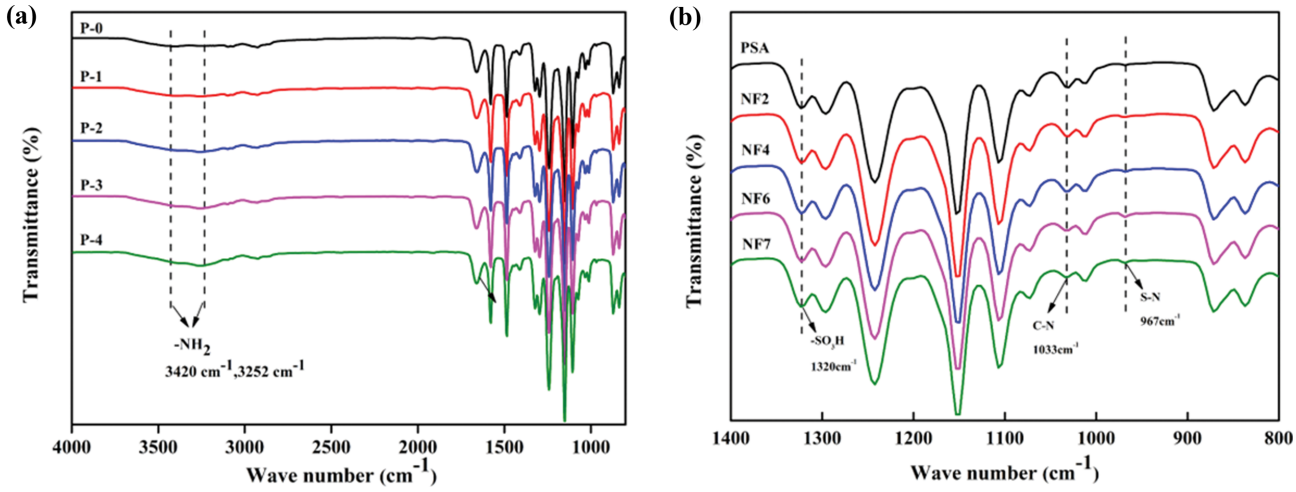


Fig. 7. ATR-FTIR spectra of the (a) P-0, P-1, P-2, P-3, and P-4 membranes; and (b) partial magnification image of (a).

sizes and a small amount of uniformly distributed pinholes before the final membrane was formed. Under such conditions, the final membrane presented fewer defects and a lower roughness.

3. Characterization of the 8-NH_2-POSS/PSA Nanocomposite Membranes

The chemical structure of the 8-NH_2-POSS/PSA nanocomposite membrane was characterized by ATR- FTIR and XPS. In addition, the influence of the 8-NH_2-POSS loading on the chemical structure of the 8-NH_2-POSS/PSA nanocomposite membrane was systematically studied. As shown in Fig. 7, the peak at 967 cm^{-1} corresponds to the stretching vibration peak of the S-N bond of the sulfonamide group [31], indicating the formation of the 8-NH_2-POSS/PSA active separation layer (Fig. 7). In addition, the peaks at 1,320 cm^{-1} and 1,033 cm^{-1} correspond to the stretching vibration peaks of the -SO_3H group of the 8-NH_2-POSS/PSA active separation layer and PES base membrane as well as the C-N bond of the macromolecular PAH, respectively (Fig. 7(a)) [31,32]. Meanwhile, the Si-O bond vibration peak of 8-NH_2-POSS at 1,080 cm^{-1} [23] was not observed (Fig. 7), which may be due to the weak signal of the Si-O bond. It is worth noting that when the content of 8-NH_2-POSS increased from 0 to 0.7 w/v%, the relative peak strength of the -NH_2 and S-N bond gradually increased, indicating that 8-NH_2-POSS not only increased the number of amino acids in the PSA active separation layer but also reacted with sulfonyl chloride during the interfacial polymerization of 8-NH_2-POSS. As a result, the degree of reaction increased at higher 8-NH_2-POSS content, which may have increased the positive charge on the surface of the 8-NH_2-POSS/PSA active separation layer and the cross-linking index of the 8-NH_2-POSS/PSA active separation layer. In addition, the effect of 8-NH_2-POSS loading on the chemical structure of 8-NH_2-POSS/PSA nanocomposite membrane was further studied by XPS. As shown in Table 2, Fig. 8, 9(b), 9(c), 9(d) and 9(e), as compared to the 8-NH_2-POSS/PSA nanocomposite membrane, Si elements were observed on the latter membrane surface, indicating that 8-NH_2-POSS was successfully introduced into the PSA membrane matrix. In addition, as the content of 8-NH_2-POSS increased, the content of elements N and S gradually increased, indicating that more amino and sulfo-

Table 2. Surface atomic content for P-0, P-1, P-2, P-3 and P-4 membranes

Membrane	C (%)	O (%)	N (%)	Si (%)	S (%)	S/N
P-0	75.86	14.52	5.72	-	3.87	0.68
P-1	72.52	16.24	5.79	1.23	4.28	0.71
P-2	70.55	17.58	5.94	1.43	4.51	0.76
P-3	68.12	17.93	6.7	1.68	5.56	0.83
P-4	67.62	18.13	6.84	1.99	5.41	0.79

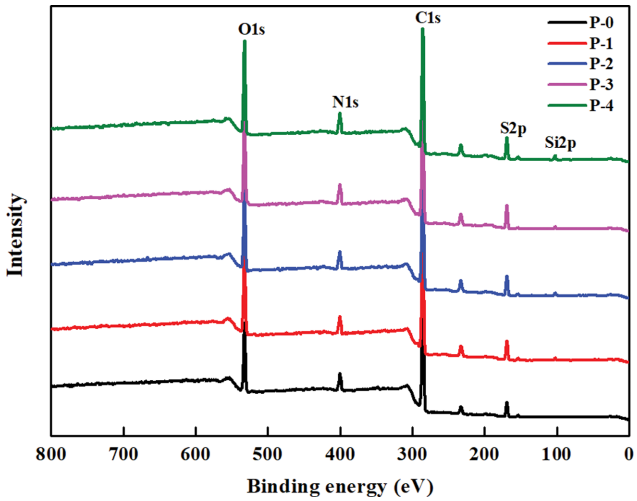


Fig. 8. XPS spectra of the P-0, P-1, P-2, P-3, and P-4 membrane surfaces.

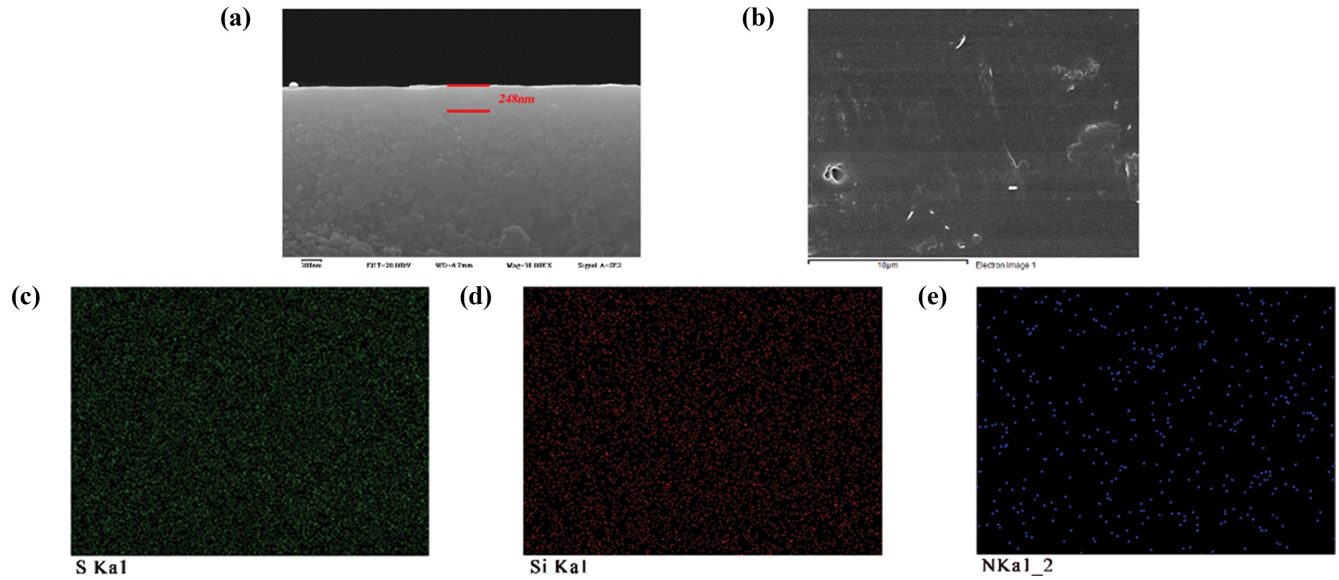


Fig. 9. (a) SEM cross-section image of the P-5 membrane; (b) TEM surface image of the P-5 membrane; (c), (d), and (e) show the S, Si, N mapping images of the P-5 membrane, respectively.

nyl chloride groups reacted in the interfacial process. This result can be attributed to the fact that 8-NH_2-POSS reacted with sulfonyl chloride groups in the interfacial polymerization process. Finally, the S/N ratio was used to analyze the effect of 8-NH_2-POSS on the crosslinking degree of the 8-NH_2-POSS/PSA nanocomposite membrane. The results showed that the order of cross-linking degree of 8-NH_2-POSS/PSA membrane was P-3>P-4>P-2>P-1>P-0. This result is consistent with the results of the membrane formation process, wherein the addition of 8-NH_2-POSS slows the interfacial polymerization reaction speed, which allows more PAH to pass through the pinhole to react with BDSC. In addition, the reduction of membrane defects was also conducive to the improvement of the cross-linking degree. However, with a significantly high 8-NH_2-POSS/PSA content (0.7 w/v%), excess 8-NH_2-POSS/PSA would agglomerate (Fig. 10(e)), which would affect the cross-linking process. In addition, to further confirm that 8-NH_2-POSS was involved in the reaction in interfacial polymerization, 8-NH_2-POSS was selected to prepare a P-5 membrane as the water phase reaction monomer and an organic phase reaction monomer BDSC. As shown in Fig. 9(a), the P-5 membrane exhibited a top layer with a thickness of 248 nm, which further indicates that 8-NH_2-POSS reacted with BDSC in interfacial polymerization.

Fig. 10 and 11 present the SEM and AFM results, respectively, wherein the 8-NH_2-POSS content exhibited a significant impact on the surface morphology and membrane thickness of the 8-NH_2-POSS/PSA nanocomposite membrane. According to Fig. 10, as the 8-NH_2-POSS content increased, P-0 to P-4 all showed a relatively smooth membrane surface. At significantly high 8-NH_2-POSS content (0.7 w/v%), some protuberances were faintly observed on the 8-NH_2-POSS/PSA nanocomposite membrane surface. This result may be due to the likely agglomeration of 8-NH_2-POSS as the 8-NH_2-POSS content increased. Furthermore, the addition of 8-NH_2-POSS resulted in the gradual increase of the membrane thickness of the 8-NH_2-POSS/PSA nanocomposite membrane; similar results were observed in previous studies [33]. The results showed that the thickness of the P-4 membrane was approximately 683 nm, which may result in more membrane resistance to the water molecules during membrane permeation, resulting in the decrease of the water permeation flux. At the same time, as the content of 8-NH_2-POSS increased, the section of the membrane still showed smooth char-

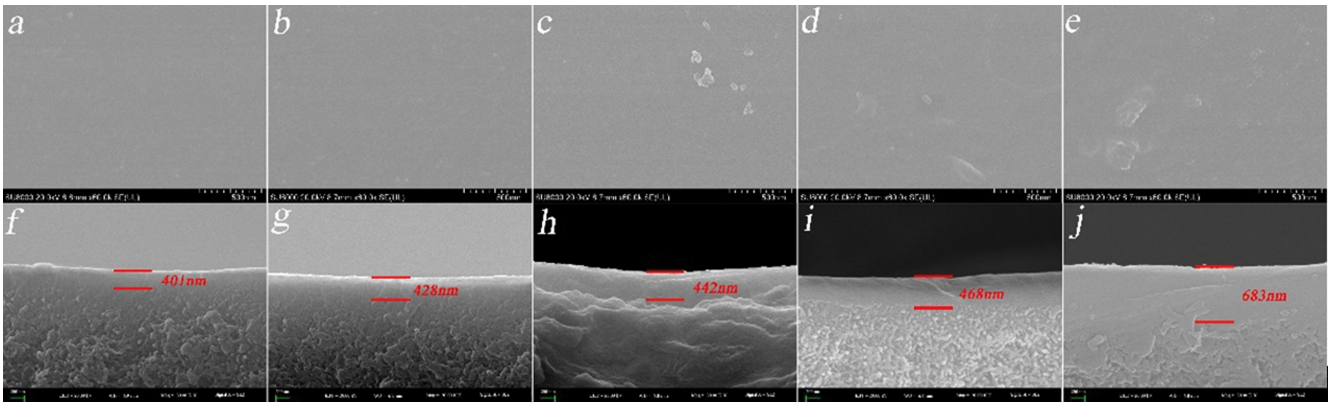


Fig. 10. SEM images (a, b, c, d, and e) show the surfaces of the P-0, P-1, P-2, P-3 and P-4 membranes, respectively. Images (f, g, h, i, and j) show the cross-sections of the P-0, P-1, P-2, P-3 and P-4 membranes, respectively.

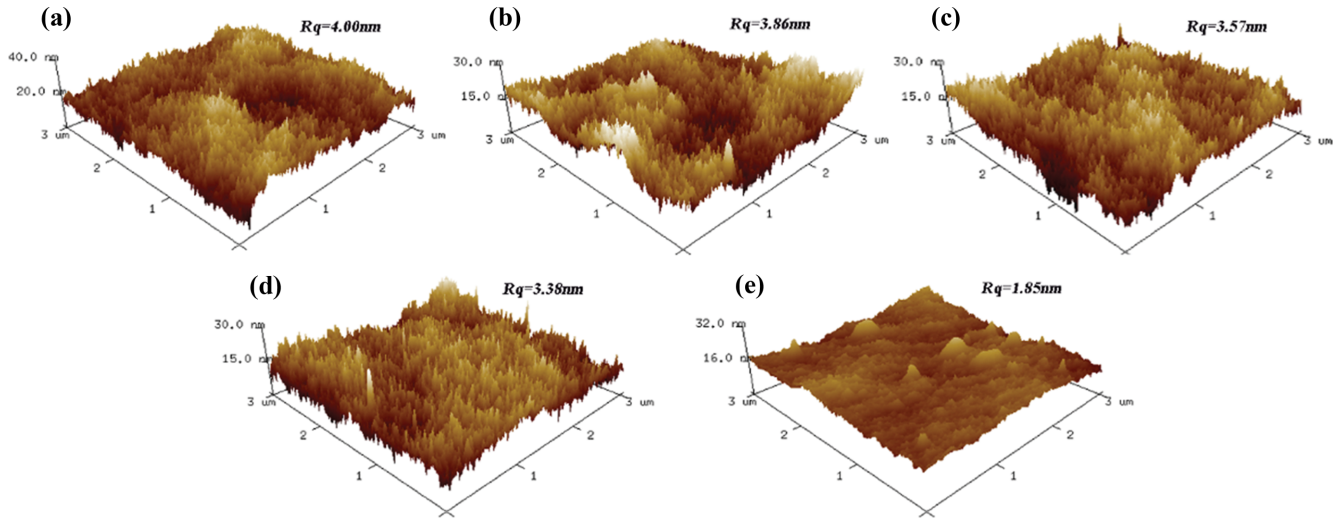


Fig. 11. Surface roughness images of the P-0, P-1, P-2, P-3, and P-4 membranes.

Table 3. PWP, Rq, WCA, SAD, and $-\Delta G_{SL}$ of the P-0, P-1, P-2, P-3, and P-4 membranes

Membrane	PWP (L/m^2 h bar)	Rq (nm)	SAD	WCA (°)	$-\Delta G_{SL}$ (mJ/m^2)
P-0	5.81	4	2.64%	87	76.5
P-1	6.86	3.86	2.66%	80	85.1
P-2	8.42	3.57	2.79%	72	94.7
P-3	10.08	3.38	2.90%	64	103.78
P-4	8.12	1.85	0.51%	61	107.9

acteristics without an obvious phase interface, indicating its good compatibility with the membrane matrix. Finally, the AFM image in Fig. 11 exhibited a decrease in the membrane surface roughness (Rq) from 4 nm to 1.85 nm as the 8-NH_2-POSS content increased from 0 to 0.7 w/v%. The result was well in line with the previously stated membrane formation process, wherein an increase in the 8-NH_2-POSS content and a decrease in the interface membrane formation rate enhanced more 8-NH_2-POSS transfer to the oil phase for participation in the reaction, thus generating a thicker membrane. In addition, all of the secondary membranes showed uniformly sized bubbles and a small amount of uniformly distributed pinholes before the final membrane was formed. Under such conditions, the final membrane exhibited fewer defects and lower roughness.

In general, the hydrophilicity and microstructure of the membrane surface affects the ability of the membrane surface to adsorb water molecules, thus affecting the membrane separation performance. Therefore, the $-\Delta G_{SL}$ (mJ/m^2) on the membrane surface free energy was used as a representative of the hydrophilic comprehensive parameters. The $-\Delta G_{SL}$ free energy of the membrane surface was calculated through Yang's-Dupre's equation [34]: $-\Delta G_{SL} = \eta'\times(1+SAD+\cos\theta)/(1+SAD)$, wherein θ defines the water contact angle (WCA), SAD defines the surface area difference (obtained from the AFM image), and η is the pure water surface tension (25 °C, 72.8 mJ/m^2). The specific values are listed in Table 3. As the 8-NH_2-POSS content increased from 0 to 0.7 w/v%, the CA of the membrane surface gradually decreased and the hydrophilicity gradually increased. At the same time, the $-\Delta G_{SL}$ (mJ/m^2) of the membrane surface gradually increased, indicating water molecule adsorption on the membrane surface. At an 8-NH_2-POSS content between 0-0.5 w/v%, the membrane surface roughness slightly reduced following a significant change in $-\Delta G_{SL}$. At this time, the 8-NH_2-POSS/PSA nanomembrane permeation flux of the water greatly improved given that the membrane surface roughness minimally affected the water flux. At an 8-NH_2-POSS content of 0.7 w/v%, the low membrane surface roughness and thick membrane thickness became the main factors hindering water transfer. In addition, the zeta potential flow meter was used to measure the membrane surface potential, "ζ", so as to further study the influence of 8-NH_2-POSS load on the surface charge properties of the 8-NH_2-POSS/PSA nanocomposite membrane. According to Fig. 12, as the content of 8-NH_2-POSS increased, the IEP on the surface of 8-NH_2-POSS/PSA nanocomposite membrane gradually increased, indicating that the positive charge on the membrane surface also gradually increased. The above results can be explained by the following facts: when 8-NH_2-POSS/PSA was introduced into the PSA membrane, part of the amino groups of 8-NH_2-POSS reacted with sulfonyl chloride, and the remaining unreacted amino groups on 8-NH_2-POSS provided hydrophilic sites in the membrane matrix to improve the hydrophilicity of the membrane surface as well as provided additional positivity sites to improve the membrane surface positivity. The excellent hydrophilic property and strong positive charge of the 8-NH_2-POSS/PSA nanocomposite membrane sur-

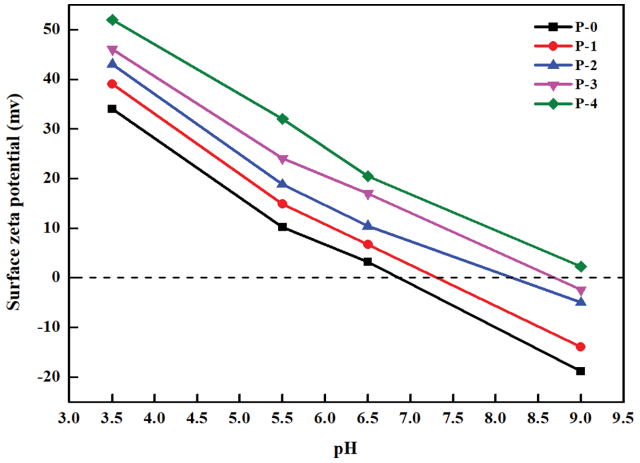


Fig. 12. Surface zeta potential of the P-0, P-1, P-2, P-3 and P-4 membranes at different pH values.

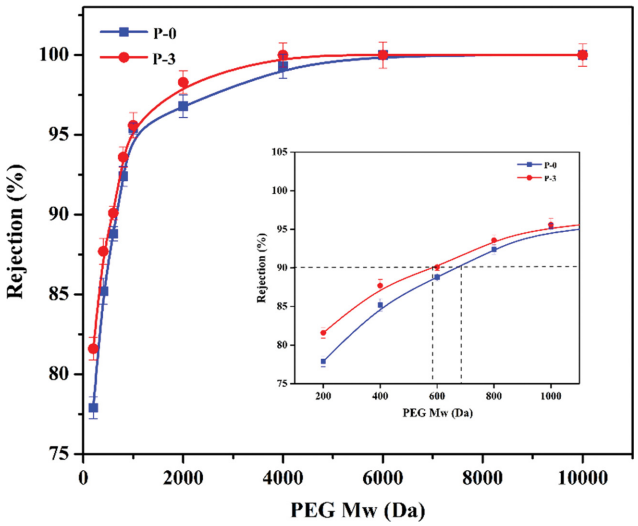


Fig. 13. PEG rejection curve for the P-0 and P-3 membranes tested with a 50 mg/L PEG solution, at 0.5 MPa, and at room temperature (25 °C).

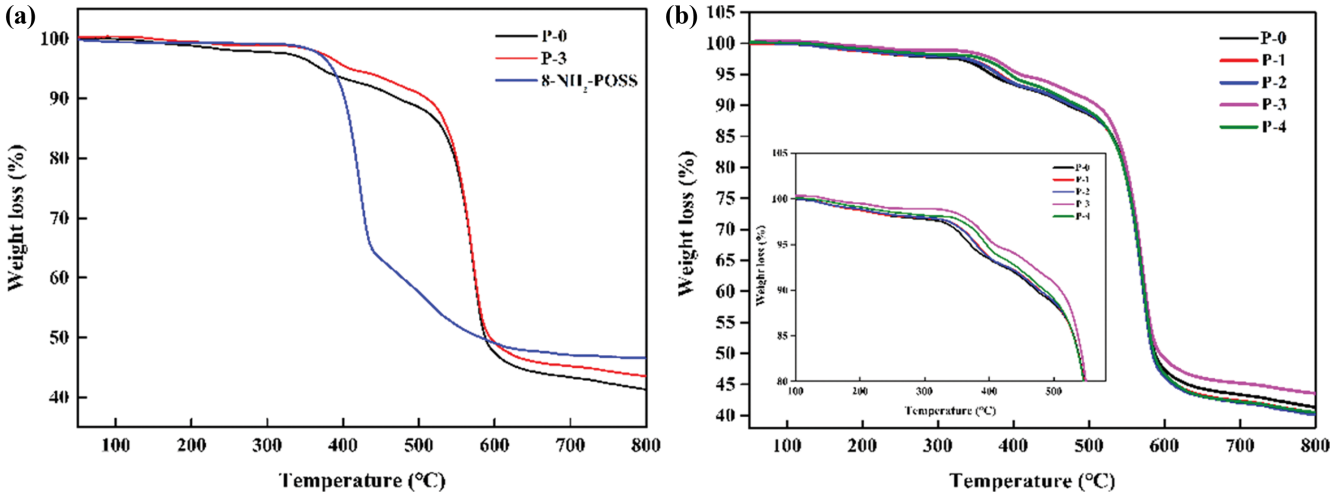


Fig. 14. TGA curves of 8-NH_2-POSS and the P-0, P-1, P-2, P-3, and P-4 membranes.

face improved the membrane separation performance and doubled the water permeability flux and salt retention rate.

Fig. 13 shows the MWCO of the P-0 and P-3 membranes. The experimental results showed that the P-0 and P-3 membranes had MWCO values of 685 Da and 580 Da, respectively. According to the DSPM model, the pore radius of the P-0 and P-3 membranes was 0.641 nm and 0.602 nm, respectively. The 8-NH_2-POSS/PSA nanocomposite membrane (P-3) was denser than the original PSA membrane (P-0), likely due to the involvement of 8-NH_2-POSS in interfacial polymerization, which improved the cross-linking degree of the 8-NH_2-POSS/PSA nanocomposite membrane. The ATR-FTIR and XPS data results also prove this point. In particular, the pore radius of P-3 membrane was larger than that of some hydration ions, such that the separation mechanism of the 8-NH_2-POSS/PSA nanocomposite membrane was mainly screened by the Donnan effect.

Finally, the thermal stability of the 8-NH_2-POSS/PSA nanocomposite membrane was characterized by TG, and the influence of 8-NH_2-POSS loading on the thermal stability of the 8-NH_2-POSS/PSA nanocomposite membrane was discussed. According to Fig. 14(a), the original PSA (P-0) membrane exhibited weight loss at about 320 °C and 570 °C, possibly due to functional group loss on the PSA membrane, such as the amino groups and the decomposition of the sulfonic acid group. In addition, 8-NH_2-POSS at 320 °C quickly decreased in weight likely due to the decomposition of the 8-NH_2-POSS amino groups. The results showed that the thermal stability of 8-NH_2-POSS was lower than that of the PSA membrane. When 8-NH_2-POSS was introduced into the PSA membrane matrix as a nanofiller, the thermal stability of the 8-NH_2-POSS/PSA nanocomposite membrane gradually increased as the content of 8-NH_2-POSS increased from 0 to 0.5 w/v% (Fig. 14(b)). As the 8-NH_2-POSS content was further increased to 0.7 w/v%, the thermal stability of P-4 membrane decreased, but was still higher than that of the P-0 membrane. This result can be explained as follows: 8-NH_2-POSS reacted with BDSC to form covalent bonds during interfacial polymerization, improving the cross-linking degree of the 8-NH_2-POSS/PSA nanocomposite membrane and the compatibility of nanomaterials with the polymer matrix. This reasoning was confirmed by the ATR-FTIR and XPS results.

4. Evaluation of the Separation Performance of the 8-NH_2-POSS/PSA Nanocomposite Membrane

The effect of 8-NH_2-POSS loading on the separation performance of the 8-NH_2-POSS/PSA nanocomposite membrane was studied. According to Figs. 2 and 3, the concentration of PAH and BDSC was fixed at 0.8 w/v% and 0.15 w/v%, respectively. An increase in the 8-NH_2-POSS content from 0 to 0.5 w/v% resulted in a gradual increase of the membrane water permeation flux and $MgCl_2$ interception rate, thus doubly increasing the water permeation flux and interception rate. At a 8-NH_2-POSS content of 0.5 w/v% (Fig. 15), optimal separation for the 8-NH_2-POSS/PSA nanocomposite membrane was observed, which exhibited a water permeation flux of 50.5 L/m^2 h and a $MgCl_2$ retention rate of 94.8%. As compared to the original PSA membrane, the water permeation flux and salt retention rate of the 8-NH_2-POSS/PSA nanocomposite membrane increased by 73.5% and 8.7%, respectively. However, as the 8-NH_2-POSS content further increased to 0.7 w/v%,

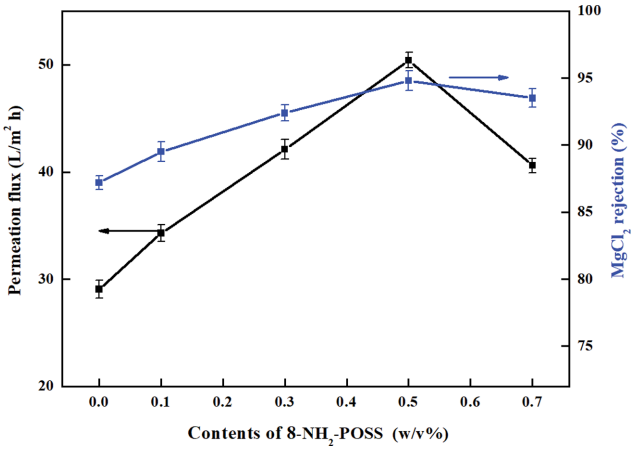


Fig. 15. Separation performance of the 8-NH_2-POSS/PSA membrane at different 8-NH_2-POSS contents.

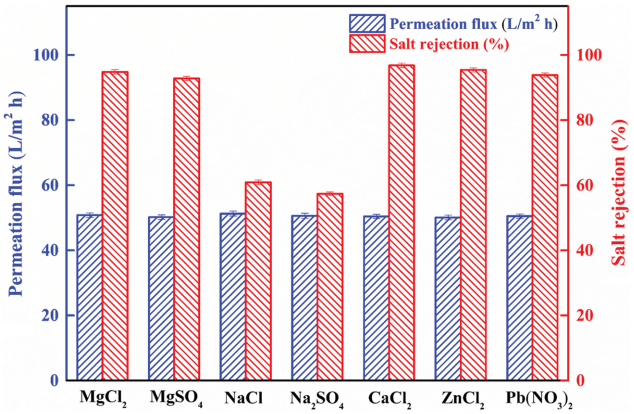


Fig. 16. Permeation flux and salt rejection of the P-3 membrane for the separation of different salts (conditions: 1 g/L aqueous solution, 25 °C).

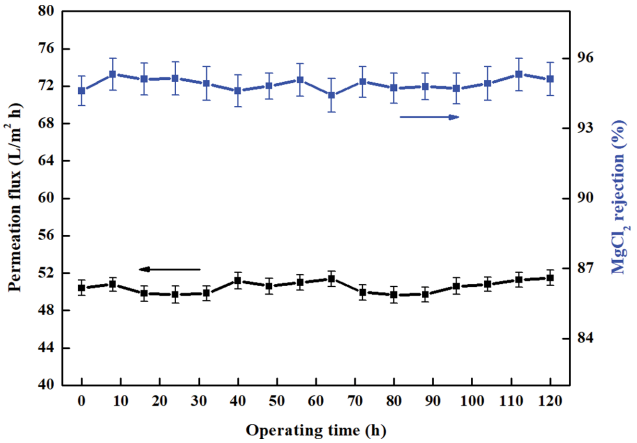


Fig. 17. Permeation flux and $MgCl_2$ rejection of the 8-NH_2-POSS/PSA nanocomposite membrane at different operation times.

the water permeation flux of the membrane decreased to 40.6 L/m^2 h and the interception rate of $MgCl_2$ slightly decreased to 93.5%. These results verify the proposed membrane formation process and characterization analyses of the 8-NH_2-POSS/PSA nanocomposite membranes very well: at increasing content of 8-NH_2-POSS (0-0.5 w/v%), the adsorption capacity of the membrane surface for water continued to increase with the increase of $-\Delta G_{SL}$. At the same time, the increasing positive charge on the membrane surface and the decreasing membrane defects resulted in a slight increase of the salt rejection rate. However, further increase of the 8-NH_2-POSS content to 0.7 w/v% resulted in 8-NH_2-POSS agglomeration, greatly reducing the membrane surface roughness and increasing the membrane thickness, which negatively impacted the membrane separation performance. According to the above experimental results, the optimal 8-NH_2-POSS content was determined to be 0.5 w/v%.

Therefore, the P-3 membrane was prepared under optimal conditions to further evaluate the separation performance of the 8-NH_2-POSS/PSA nanocomposite membrane. Fig. 16 shows the interception rate of the P-3 membrane against seven salts: $CaCl_2$ (96.8%)> $ZnCl_2$ (95.1%)≈$MgCl_2$ (94.8%)>$Pb(NO_3)_2$ (93.8%)>$MgSO_4$ (92.8%)> NaCl (60.9%)>Na_2SO_4 (57.4%). However, no obvious water permeation flux change was observed. According to the previous discussion, the separation mechanism of the P-3 membrane only considered the Donnan effect. The strength of the Donnan effect is related to the valence state and diffusion coefficient of the separated ions. In general, the interception rate of the positively charged NF membranes on bivalent metal ion salts is higher than that of univalent metal ion salts: $MgCl_2$>NaCl. For salts containing the same valence ions (Ca^{2+}, Zn^{2+}, Mg^{2+}, Pb^{2+}), the interception rate was determined by the diffusion coefficient of the metal ions. In general, lower metal ion diffusion coefficients increase the difficulty in passing through the membrane, thereby producing a higher retention rate. The order of diffusion coefficients is shown in the table: Ca^{2+}<Zn^{2+}<Mg^{2+}<Pb^{2+}, wherein the interception rate was determined to be $CaCl_2$>$ZnCl_2$≈$MgCl_2$>$Pb(NO_3)_2$. In conclusion, the 8-NH_2-POSS/PSA nanocomposite membrane is very suitable for water softening and the treatment of wastewater containing divalent metal ions or heavy metal ions.

In practical applications, long-term operational stability is essential for the application of nanocomposite membranes [17]. Poor compatibility between the nanofillers and the polymer matrix may result in nanofiller detachment during the separation process and membrane structure damage, which will eventually lead to the rapid deterioration of the membrane separation performance. Therefore, long-term membrane stability evaluation is necessary. The long-term operational stability of the prepared 8-NH_2-POSS/PSA nanocomposite membrane was evaluated by a continuous nanofiltration test (120 h). According to Fig. 17, the water permeability flux and the $MgCl_2$ interception rate of the P-3 membrane slightly changed, indicating that the membrane has good long-term performance and stability. This may be a result of covalent bonding between 8-NH_2-POSS and the PSA membrane matrix, which improved the interaction between 8-NH_2-POSS and the PSA membrane matrix and ultimately enhanced the stability of the membrane structure.

The acid stability of the nanofiltration membrane is an important parameter in the treatment of industrial wastewater containing divalent metals, heavy metal ions, or various strongly acidic substances. The P-3 membrane was immersed in 20.0 w/v% H_2SO_4 solution for the acid stability test. SEM was used to observe any change in the P-3 membrane surface before and after immersion of acid solution for 30 days (Fig. 18). No obvious cracks were observed on the P-3 membrane surface after immersion in the acidic solution. In addition, ATR-FTIR analysis was performed to characterize any change in the P-3 membrane surface chemical structure before and after 30 days of immersion in the acid solution. According to Fig. 19, the S-N peak that was observed at 967 cm^{-1} on the surface of the P-3 membrane was still present in the infrared spectrum of the membrane surface 30 days after immersion in the acidic solution. Fig. 20 presents the separation performance of the P-3 membrane after immersion in the acidic solution for a period of time. As the immersion time of the P-3 membrane in the acidic solution increased to 30 days, the retention rate of $MgCl_2$ decreased from 94.8% to 91.8%, and the corresponding permeation flux increased from 50.6 L/m^2 h to 54.7 L/m^2 h. The results show that the separation performance of the P-3 membrane minimally changed after immersion in the acid solution and still showed good separa-

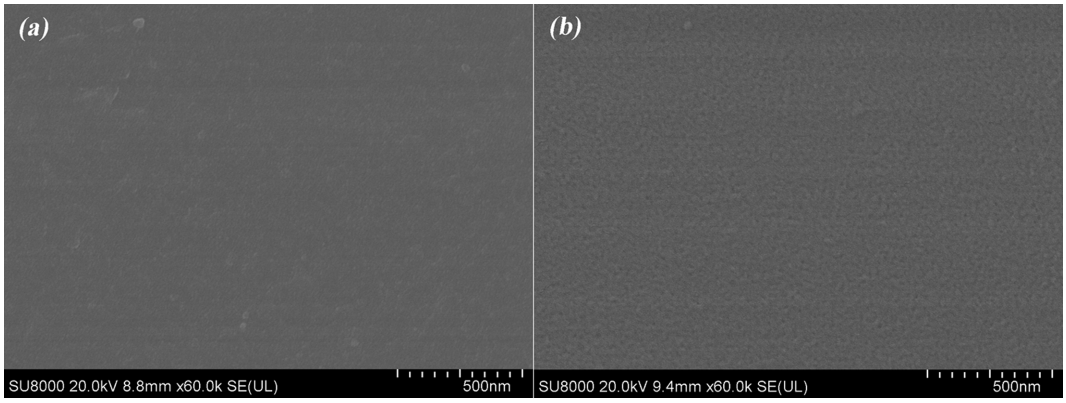


Fig. 18. SEM images of the (a) P-3 membrane surface and (b) P-3 membrane surface after exposure to an acid solution for 30 days.

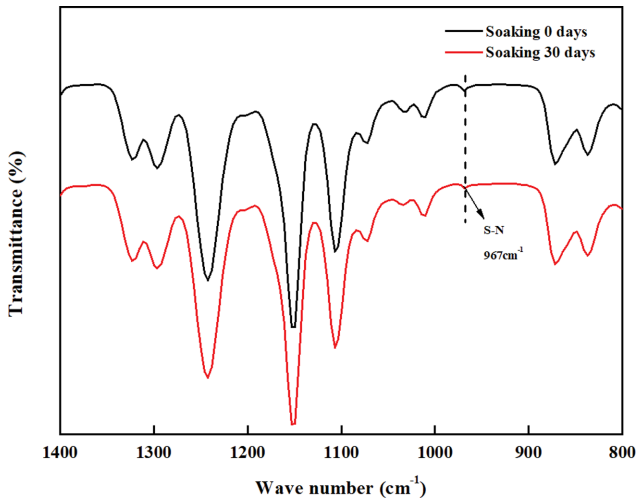


Fig. 19. ATR-FTIR spectra of the P-3 membrane after exposure to an acidic solution for 0 and 30 days.

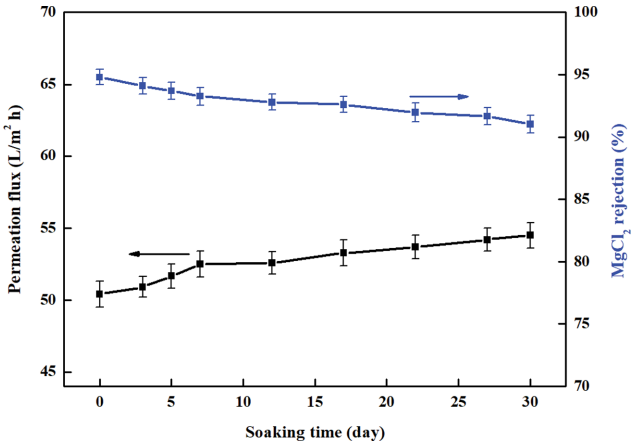


Fig. 20. Separation performance of the 8-NH_2-POSS/PSA membrane after exposure to 20 w/v% H_2SO_4 solutions for a fixed period (conditions: 1 g/L $MgCl_2$ solution, 0.5 MPa, pH 6.5, and room temperature (25 °C)).

Table 4. Comparisons of the separation performance of the 8-NH_2-POSS/PSA nanocomposite membrane prepared in this work with other TFC NF membranes

Membrane materials	Salt rejection (%)	Permeate flux (L/m^2 h bar)	Testing conditions	Ref.
PIP-NTSC	70.8%[b]	5.72	20.0% (w/v) H_2SO_4, 25 °C cross-flow filtration setup	[35]
DMAP/TMC	83.9%[b]	6.0	pH 7.4, 25 °C, cross-flow filtration setup	[36]
HPEI/MWCNT(M8)	89.3%[a]	7.7	pH 6, 25 °C cross-flow filtration setup	[37]
TFN (ZIF-8@PDA PEI/TMC)	95.8%[a]	6.0	pH 6.5, 25 °C, cross-flow filtration setup	[38]
Quaternized polyelectrolyte complex membranes	95.7%[a]	6.4	pH 6.5, 25 °C, cross-flow filtration setup	[39]
8-HQ/Fe_3O_4 NPs	96.0%[b]	4.3	25 °C, dead-end filtration setup	[40]
HPEI/MWCNT(M6)	97.3%[a]	7.2	pH 6, 25 °C cross-flow filtration setup	[37]
Polysulfonamide (PAH-BDSC)	88.3%[a]	7.8	20.0% (w/v) H_2SO_4, 25 °C cross-flow filtration setup	[31] our previous work
8-NH_2-POSS/PSA composite membrane	94.8%[a]	10.5	20.0% (w/v) H_2SO_4, 25 °C cross-flow filtration setup	This work

[a]Separation performance with $MgCl_2$ solution.
[b]Separation performance with $MgSO_4$ solution.

tion performance. These results indicate that the 8-NH_2-POSS/PSA nanocomposite membrane has excellent acid stability. In addition, Table 4 exhibits a comparison of the NF performance between 8-NH_2-POSS/PSA nanocomposite membranes in this work and other TFC NF membranes. It can be observed that the 8-NH_2-POSS/PSA nanocomposite membrane fabricated in this study possesses higher permeation and qualified selectivity against divalent magnesium salt solutions.

CONCLUSIONS

The OM method was introduced to study the effect of the 8-NH_2-POSS nanoparticles on the IP nanocomposite membrane formation process. Stronger interaction between the PAH molecules and 8-NH_2-POSS nanoparticles increased the surface tension of the water phase and reduced the mass transfer rate of the PAH molecules to the oil phase. The increase in the interfacial tension between the nascent membrane and organic phase reduced the instability of the nascent membrane, thus dampening the formation of evenly distributed pinholes on the nascent membrane and ultimately producing fewer defects and lower roughness on the final membrane. The 8-NH_2-POSS content in the water phase likely influenced the membrane separation layer thickness and roughness. The excellent hydrophilic property and strong positive charge of the 8-NH_2-POSS/PSA nanocomposite membrane surface improved the membrane separation performance. The 8-NH_2-POSS/PSA nanocomposite membrane (0.5 w/v%) exhibited the best performance with a high $MgCl_2$ rejection rate of 94.8% and a high water permeation flux of 50.5 L/m^2 h of 0.5 MPa. Meanwhile, the 8-NH_2-POSS/PSA nanocomposite membrane illustrated its excellent chemical stability in an acidic environment. In particular, the above findings provide theoretical guidance for the controlled preparation of the NF membrane.

ACKNOWLEDGEMENTS

The financial support for this work is from the National Natural Science Foundation of China (No. 21464012), the funds for dual first-class discipline of Shihezi university (SHYL-YB201806), the funds for innovation and development of Shihezi university (CXFZ201909), the Program for Changjiang Scholars and Innovative Research Team in University (No. IRT_15R46) and Bingtuan Innovation Team in Key Areas (2015BD003).

REFERENCES

1. G. S. Lai, W. J. Lau, P. S. Goh, A. F. Ismail, H. Y. Tan, Y. C. Chong, R. K. Rehberg and S. Awad, *Chem. Eng. J.*, **344**, 524 (2018).
2. Y. Zhang, Y. L. Su, J. M. Peng, X. T. Zhao, J. Z. Liu, J. J. Zhao and Z. Y. Jiang, *J. Membr. Sci.*, **429**, 235 (2013).
3. Z. W. Lv, J. H. Hu, J. F. Zheng, X. Zhang and L. J. Wang, *Ind. Eng. Chem. Res.*, **55**, 4726 (2016).
4. G. H. Liu, Z. Y. Jiang, X. X. Cheng, C. Chen, H. Yang, H. Wu, F. S. Pan, P. Zhang and X. Z. Cao, *J. Membr. Sci.*, **520**, 364 (2016).
5. H. Y. Wang, C. L. Wu, Z. Wei, C. Li and Q. Liu, *RSC Adv.*, **6**, 4673 (2016).
6. X. Jiang, S. W. Li, S. S. He, Y. P. Bai and L. Shao, *J. Mater. Chem. A.*, **6**, 15064 (2018).
7. Y. L. Ji, Q. F. An, F. Y. Zhao and C. J. Gao, *Desalination*, **357**, 8 (2015).
8. Y. F. Li, Y. L. Su, Y. A. Dong, X. T. Zhao, Z. Y. Jiang, R. N. Zhang and J. J. Zhao, *Desalination*, **333**, 59 (2014).
9. Y. J. Tang, Z. L. Xu, S. M. Xue, Y. M. Wei and H. Yang, *J. Membr. Sci.*, **498**, 374 (2016).
10. Z. P. Liao, X. F. Fang, J. Xie, Q. Li, D. P. Wang, X. Y. Sun, L. J. Wang and J. S. Li, *ACS Appl. Mater. Interfaces*, **11**, 5344 (2019).
11. H. Z. Zhang, Z. L. Xu, H. Ding and Y. J. Tang, *Desalination*, **420**, 158 (2017).
12. B. H. Jeong, E. M. V. Hoek, Y. Yan, A. Subramani, X. Huang, G. Hurwitz, A. K. Ghosh and A. Jawor, *J. Membr. Sci.*, **294**, 1 (2007).
13. P. G. Ingole, M. I. Baig, W. Choi, X. H. An, W. K. Choi and H. K. Lee, *J. Ind. Eng. Chem.*, **48**, 5 (2017).
14. K. T. Cao, Z. Y. Jiang, J. Zhao, C. H. Zhao, C. Y. Gao, F. S. Pan, B. Y. Wang, X. Z. Cao and J. Yang, *J. Membr. Sci.*, **469**, 272 (2014).
15. M. Moochani, A. Moghadassi, S. M. Hosseini, E. Bagheripour and F. Parvizian, *Korean J. Chem. Eng.*, **33**, 2674 (2016).
16. S. M. Xue, Z. L. Xu, Y. J. Tang and C. H. Ji, *ACS Appl. Mater. Interfaces*, **8**, 19135 (2016).
17. J. Y. Zhu, L. J. Qin, A. Uliana, J. W. Hou, J. Wang, Y. T. Zhang, X. Li, S. S. Yuan, J. Li, M. M. Tian, J. Y. Lin and B. V. D. Bruggen, *ACS Appl. Mater. Interfaces*, **9**, 1975 (2017).
18. C. B. Wang, Z. Y. Li, J. X. Chen, Z. Li, Y. H. Yin, L. Cao, Y. L. Zhong and H. Wu, *J. Membr. Sci.*, **523**, 273 (2017).
19. M. T. Hoang, T. D. Pham, D. Verheyen, M. K. Nguyen, T. T. Pham, J. Y. Zhu and B. V. Bruggen, *Chem. Eng. Sci.*, **228**, 115998 (2020).
20. N. Izadmehr, Y. Mansourpanah, M. Ulbricht, A. Rahimpour and M. R. Omidkhah, *J. Environ. Manage.*, **276**, 111299 (2020).
21. F. Yuan, Z. Wang, X. W. Yu, Z. H. Wei, S. C. Li, J. X. Wang and S. C. Wang, *J. Phys. Chem. C.*, **116**, 11496 (2012).
22. J. T. Duan, E. Litwiller and I. Pinnau, *J. Membr. Sci.*, **473**, 157 (2015).
23. X. D. You, T. Y. Ma, Y. L. Su, H. Wu, M. Y. Wu, H. W. Cai, G. M. Sun and Z. Y. Jiang, *J. Membr. Sci.*, **540**, 454 (2017).
24. S. Bandehali, A. Moghadassi, F. Parvizian and S. M. Hosseini, *Korean J. Chem. Eng.*, **36**, 1657 (2019).
25. K. P. Lee, G. Bargeman, R. D. Rooij, A. J. B. Kemperman and N. E. Benes, *J. Membr. Sci.*, **523**, 487 (2017).
26. K. P. Lee, J. M. Zheng, G. Bargeman, A. J. B. Kemperman and N. E. Benes, *J. Membr. Sci.*, **478**, 75 (2015).
27. A. D. Sabde, M. K. Trivedi, V. Ramachandhran, M. S. Hanra and B. M. Misra, *Desalination*, **114**, 223 (1997).
28. M. H. Liu, G. H. Yao, Q. B. Cheng, M. Ma, S. C. Yu and C. J. Gao, *J. Membr. Sci.*, **415**, 122 (2012).
29. A. K. Ghosh, B. H. Jeong, X. F. Huang and E. M. V. Hoek, *J. Membr. Sci.*, **311**, 34 (2008).
30. Z. W. Thong, Y. Cui, Y. K. Ong and T. S. Chung, *ACS Sustain. Chem. Eng.*, **4**, 5570 (2016).
31. H. Wang, Z. Wei, H. Y. Wang, H. J. Jiang, Y. C. Li and C. L. Wu, *RSC Adv.*, **9**, 2042 (2019).
32. J. J. Richardson, B. L. Tardy, H. Ejima, J. L. Guo, J. W. Cui, K. Liang, G. H. Choi, J. P. Yoo, B. G. D. Geest and F. Caruso, *ACS Appl. Mater. Interfaces*, **8**, 7449 (2016).
33. Y. R. He, Y. P. Tang and T. S. Chung, *Ind. Eng. Chem. Res.*, **55**, 12929 (2016).

34. F. Y. Zhao, Y. L. Ji, X. D. Weng, Y. F. Mi, C. C. Ye, Q. F. An and C. J. Gao, *ACS Appl. Mater. Interfaces*, **8**, 6693 (2016).
35. M. H. Liu, G. H. Yao, Q. B. Cheng, M. Ma, S. C. Yu and C. J. Gao, *J. Membr. Sci.*, **415**, 122 (2012).
36. R. J. Zhang, S. L. Yu, W. X. Shi, W. Wang, X. Y. Wang, Z. Q. Zhang, L. Lia, B. Zhang and X. Bao, *J. Membr. Sci.*, **542**, 68 (2017).
37. M. Peydayesh, T. Mohammadi and O. Bakhtiari, *J. Ind. Eng. Chem.*, **69**, 127 (2019).
38. M. Qiu and C. J. He, *J. Hazard. Mater.*, **367**, 339 (2018).
39. C. C. Ye, Q. F. An, J. K. Wu, F. Y. Zhao, P. Y. Zheng and N. X. Wang, *Chem. Eng. J.*, **359**, 994 (2018).
40. S. Ansari, A. Moghadassi and S. M. Hosseini, *Korean J. Chem. Eng.*, **37**, 2011 (2020).